Journal of Power Sources 223 (2013) 100–106

Contents lists available at SciVerse ScienceDirect

Journal of Power Sources

journal homepage: www.elsevier.com/locate/jpowsour

High-performance $LiFePO_4$ cathode material from $FePO_4$ microspheres with carbon nanotube networks embedded for lithium ion batteries

Meng Chen [a], Chunyu Du [b,*], Bai Song [a], Kai Xiong [b], Geping Yin [b], Pengjian Zuo [b], Xinqun Cheng [b]

[a] School of Chemistry and Materials Science, Harbin Engineering University, 150080 Harbin, PR China
[b] School of Chemical Engineering and Technology, Harbin Institute of Technology, 150001 Harbin, PR China

HIGHLIGHTS

- Porous $FePO_4$ microspheres with uniform carbon nanotube (CNT) embedded are prepared by a hydrothermal process.
- $LiFePO_4$ microspheres with CNT networks ($LiFePO_4$/CNT) are obtained and tested as the cathode material for lithium ion batteries.
- Our $LiFePO_4$/CNT material displays both excellent volumetric Li storage properties and stable charge/discharge cyclability.

GRAPHICAL ABSTRACT

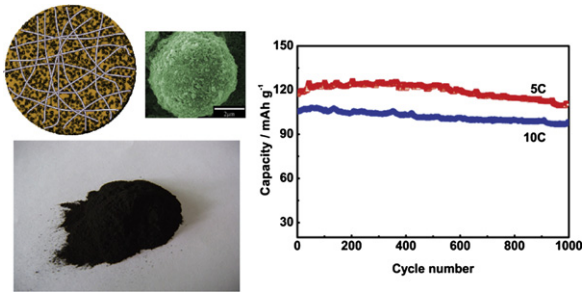

ARTICLE INFO

Article history:
Received 1 July 2012
Received in revised form
12 September 2012
Accepted 13 September 2012
Available online 21 September 2012

Keywords:
Lithium ion batteries
Cathode material
Lithium iron phosphate
Carbon nanotube
Hydrothermal process

ABSTRACT

This paper reports a facile approach to prepare $FePO_4$ microspheres with carbon nanotube embedded ($FePO_4$/CNT) by a hydrothermal process, from which $LiFePO_4$/CNT microspheres were further obtained by chemical lithiation. The preparation procedure is simple, well reproducible, and easy to be scaled up. In addition to the desirable spherical morphology that leads to high tap density, these microspheres contain uniform and well-connected CNT networks, which remarkably enhances their electronic conductivity. Meanwhile, these materials develop a large amount of nanopores during the synthesis, giving rise to both large surface area and good electrolyte infiltration. The $LiFePO_4$/CNT material displays both excellent volumetric Li storage properties at high current rates (>155 mAh cm^{-3} at 5C), and stable charge/discharge cyclability (>90% capacity retention after 1000 charge/discharge cycles). The $LiFePO_4$/CNT microspheres are rather promising for high-power lithium ion batteries, and such an approach can be extended to prepare other high-performance electrode materials.

1. Introduction

Olivine-type lithium iron phosphate ($LiFePO_4$) has recently received substantial interest as one of the most promising cathode materials for Li-ion batteries (LIBs), because of its low cost, environmental compatibility, superior capacity retention, thermal stability and safety [1–4]. However, the poor electronic conductivity of pure $LiFePO_4$ phase leads to the significantly low rate performance, which has become a bottleneck for its wide commercialization, especially for high power applications [5–7]. To circumvent this main drawback, numerous efforts have been made, including metallic cation doping [8,9], carbon coating [10,11], and reduction of the particle size to nanoscale [12,13]. Among them, synthesizing nanosized $LiFePO_4$ particles seems to be highly efficient, because the path length of electron transport is greatly minimized and the effective active surface area is remarkably increased [14–17].

* Corresponding author. Tel.: +86 451 86403216; fax: +86 451 86418616.
E-mail address: cydu@hit.edu.cn (C. Du).

0378-7753/$ – see front matter © 2012 Elsevier B.V. All rights reserved.
http://dx.doi.org/10.1016/j.jpowsour.2012.09.040

Unfortunately, although nanosized $LiFePO_4$ particles have shown enhanced electronic conductivity and thus improved rate performance, their tap density is dramatically reduced, giving rise to the low volumetric energy density. Furthermore, the nanosized $LiFePO_4$ particles cause difficulties in the electrode fabrication process, which mainly involves the inhomogeneous mixing and coating of the electrode slurry, resulting in the peeling-off of electrode materials from the current collector. In contrast to nanosized $LiFePO_4$ particles, microsized $LiFePO_4$ spheres ($LiFePO_4$ microspheres) are easy to form closely packed arrays, and good for improving the volumetric energy density [18,19]. In addition, $LiFePO_4$ microspheres have better fluidity characteristics, which is apparently beneficial to the electrode fabrication process. Nevertheless, it was reported that the $LiFePO_4$ microspheres synthesized by a co-precipitation method exhibited relatively low discharge capacity and rate performance [20,21], which was mainly attributed to their poor electronic conductivity so that a large amount of $LiFePO_4$ at the center of the microspheres could not be efficiently utilized [22,23]. Therefore, it is desirable to synthesize $LiFePO_4$ microspheres with greatly improved electronic conductivity for achieving both high volumetric energy density and good rate capability.

In this paper, we report a novel approach to synthesize the porous $FePO_4$ and carbon nanotube ($FePO_4$/CNT) composite microspheres, by which CNT as a highly conductive component is in-situ and uniformly embedded into the $FePO_4$ microspheres to form a conductive CNT network. Using the $FePO_4$/CNT microspheres as the precursor, $LiFePO_4$/CNT microspheres were easily obtained by a chemical lithiation process. Our results provide a facile approach for simultaneously achieving the microspherical morphology and excellent electronic conductivity for the $FePO_4$ and $LiFePO_4$ material. Thus obtained $LiFePO_4$/CNT microspheres exhibit greatly increased volumetric energy density, good rate capability and superior cyclability, which is promising as the high-performance cathode material for LIBs.

2. Experimental

2.1. Synthesis of the $FePO_4$/CNT and $LiFePO_4$/CNT microspheres

Iron phosphate microspheres embedded with an uniform CNT network ($FePO_4$/CNT) as the precursor were facilely synthesized by an in-situ CNT-embedding approach with $Fe(NO_3)_3$, $NH_4H_2PO_4$ and CNT as the starting materials. Specifically, to 40 ml of 0.5 M $Fe(NO_3)_3$ solution, an equimolar solution of $NH_4H_2PO_4$ was added dropwise in the 1:1 volume ratio under vigorous stirring. Then, 15 ml of aqueous dispersion of multi-walled CNTs, which were pretreated according to the previously reported procedure [24], was injected to form a suspension. After stirring for 2 h, 1 M ammonia solution was added to adjust pH value of the suspension to 1.5. Subsequently, the suspension was transferred into a Teflon-lined autoclave and heated at 150 °C for 12 h. After the hydrothermal reaction ceased, the $FePO_4$/CNT precipitate was collected on a membrane filter, washed several times with deionized water, and dried in oven at 80 °C for 24 h.

The $LiFePO_4$/CNT microspheres were obtained by chemical lithiation of the $FePO_4$/CNT precursor at high temperatures with sucrose served as the carbon source, which was similar to the previous procedures [25,26]. Briefly, the $FePO_4$/CNT precursor was suspended in aqueous solution of LiOH and sucrose with the molar ratio of 1:1:0.075. The suspension was vigorously stirred for 2 h at room temperature. After that, water in the suspension was completely evaporated at 80 °C. Finally, the resulting mixture was calcined in a tubular furnace at 650 °C for 15 h under reducing atmosphere (Ar/H_2 in 95/5) to obtain the $LiFePO_4$/CNT microspheres. For comparison, pure $LiFePO_4$ microspheres were also synthesized following the above procedure except that no CNT was added.

2.2. Characterization

The crystalline phase of resulting samples was characterized by powder X-ray diffraction (XRD) using a Rigaku D/max-rA diffractometer with Cu Kα radiation. The morphology of samples was determined by field emission scanning electron microscopy (FE-SEM) at 20 kV on a JEM 100CX-II microscope equipped with an energy dispersion X-ray spectroscopy (EDX) device. To measure the tap density, a certain amount of the $LiFePO_4$ samples were placed in a small measuring cylinder and tapped for 10 min. The measured volume of the tapped powders and their mass were used to calculate the tap density. The electrical conductivities were measured by using a standard four-point probe method. The samples were prepared by a cold-press method with an applied pressure of 60 MPa and a duration time of 10 min.

The electrochemical performance of the $LiFePO_4$/CNT composite microspheres was tested using a CR2025-type coin cell. To prepare the working electrodes, the active material powder, carbon black and poly(vinylidene fluoride) binder were mixed at a weight ratio of 80:10:10 in *N*-methyl-2-pyrrolidone solvent. The mixed viscous slurry was cast onto Al foil and dried at 80 °C under vacuum for 12 h. The obtained film was cut into circular discs with area of ~1.5 cm^2, and the discs were pressed at a pressure of 10 MPa to use as the working electrodes. The working electrodes with approximately 2.3 mg of the active materials were assembled in coin cells with a lithium metal foil as the counter electrode, a Celgard 2400 film as the separator, and 1.0 M $LiPF_6$ solution in ethylene carbonate, diethyl carbonate and dimethyl carbonate (1:1:1, in volume) as the electrolyte. The electrode performance was investigated in terms of charge/discharge curves and cycling capacity using a NEWARE battery-testing system (Neware Co., Ltd., China) at the cut-off voltages of 2.5 and 4.2 V. Electrochemical impedance spectroscopy (EIS) was measured using CHI604D (CH Instruments, China). The amplitude of the AC signal was 5 mV over the frequency range between 1×10^5 and 0.01 Hz. All the electrochemical measurements were carried out at room temperature, and the potentials were given with respect to Li^+/Li .

3. Results and discussion

The porous $FePO_4$/CNT microspheres with uniform CNT networks embedded were prepared by the in-situ hydrothermal growth, and the $LiFePO_4$/CNT microspheres were further obtained by a high-temperature chemical lithiation process. The synthetic mechanism is schematically demonstrated in Fig. 1. In brief, Fe^{3+} ions dissolved in the solution were first anchored on CNT surfaces by the electrostatic interaction between Fe^{3+} ions and the negatively charged CNT surfaces that were developed by refluxing CNT in strong acid solutions. After that, $FePO_4$ nanoparticles were formed on the CNT surfaces by adjusting pH value of the solution to reduce the $FePO_4$ solubility. During the subsequent hydrothermal process, the $FePO_4$ nanoparticles grew and were assembled into porous microspheres with CNT simultaneously embedded, which is necessary for reducing the surface tension of the dispersed particles. The $FePO_4$/CNT spherical precursor was finally transformed to $LiFePO_4$/CNT microspheres by a chemical lithiation process at high temperatures.

To follow the synthesis, morphologies of the $FePO_4$/CNT and $LiFePO_4$/CNT samples were examined by SEM. As shown in Fig. 2A, most of the $FePO_4$/CNT particles were perfect microspheres with the diameter of 4–6 μm. Furthermore, no apparent CNTs could be detected, indicating that the CNTs had been successfully

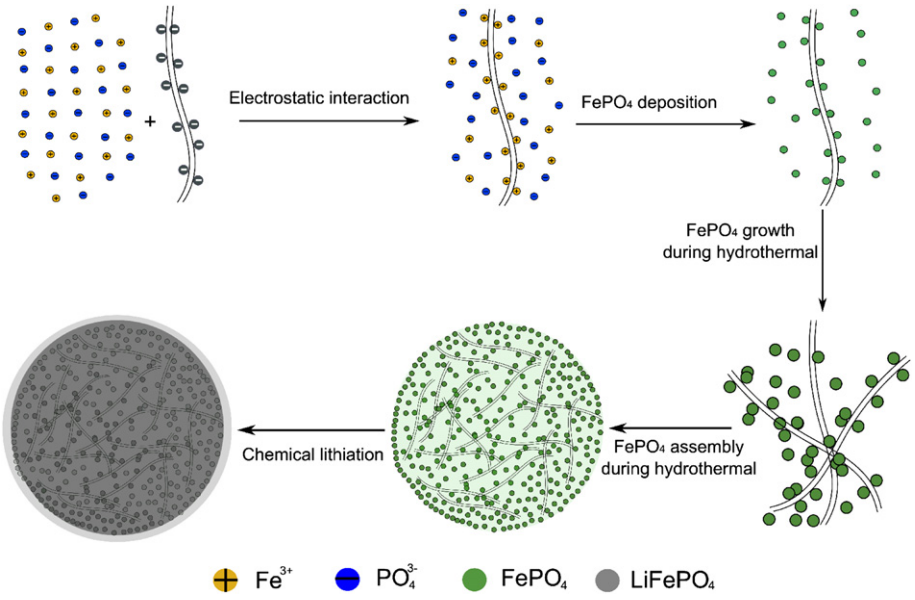

Fig. 1. Schematic illustration of the synthesis of the $FePO_4$/CNT and $LiFePO_4$/CNT microspheres.

incorporated into the $FePO_4$ microspheres since the supernatant after the hydrothermal process was completely clear and did not contain any CNT. From the magnified image (inset of Fig. 2A), it was evident that the $FePO_4$/CNT microsphere was composed of numerous nanoparticles, and these nanoparticles were interconnected together to form a porous structure with the pore size of 5–20 nm. Meanwhile, a few CNTs (indicated by circle) were still found to protrude from surface of the microsphere, confirming the incorporation of CNTs into the $FePO_4$ microspheres. Such a porous and CNT-embedded structure was expected to simultaneously facilitate the electrolyte penetration and the electronic conductivity, thus leading to improved rate performance.

To examine whether CNTs were uniformly dispersed in the $FePO_4$/CNT microsphere, we carried out EDX and elemental

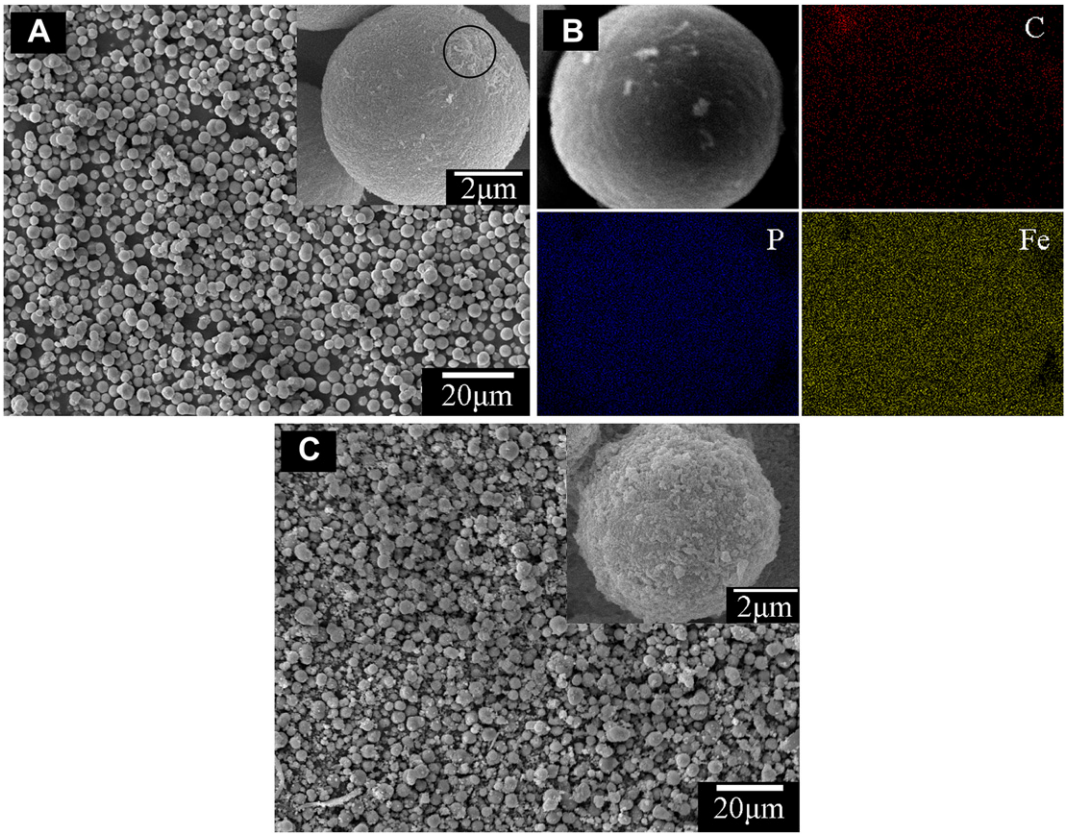

Fig. 2. (A) SEM image and (B) elemental mapping of the $FePO_4$/CNT precursor, and (C) SEM image of the $LiFePO_4$/CNT microspheres. Insets: Magnified SEM images.

mapping characterization. The EDX result revealed that the Fe/P molar ratio of the $FePO_4$/CNT microspheres was close to 1.0, suggesting the formation of $FePO_4$ by the hydrothermal process. Moreover, it was found that the $FePO_4$/CNT microspheres contained ~1.5 wt% of C, which was roughly in agreement with the original feed ratio before the hydrothermal process. From the elemental mapping images of Fe, P and C for a typical $FePO_4$/CNT microsphere (Fig. 2B), not only were the elements of Fe and P homogeneously distributed, but also the C element was continuous and even in the whole $FePO_4$/CNT microsphere, indicating the formation of a uniform three-dimensional CNT network.

After the chemical lithiation process, the morphology and particle size of thus obtained $LiFePO_4$/CNT microspheres (Fig. 2C) were in general similar to those of the $FePO_4$/CNT precursor, although there were a small amount of nanosized particles observed, which might be amorphous carbon pyrolyzed from sucrose or $LiFePO_4$ nanoparticles detached from the microspheres during the chemical lithiation. This result clearly indicated that the chemical lithiation process did not significantly damage the spherical morphology, and our approach was a facile route to synthesize the $LiFePO_4$/CNT composite microspheres. Also, compared with the $FePO_4$/CNT precursor, both the particle and pore sizes of the $LiFePO_4$/CNT microspheres became a little larger, which was apparently due to the volume expansion from $FePO_4$ to $LiFePO_4$. Such an increase in pore size, confirmed by the pore size distribution curves of $FePO_4$/CNT and $LiFePO_4$/CNT materials (Fig. 3), leads to better electrolyte penetration, and thus higher rate performance.

In order to reveal the formation mechanism of the $FePO_4$/CNT and $LiFePO_4$/CNT composite microspheres, the $FePO_4$ and $LiFePO_4$ materials without the incorporation of CNT were also synthesized. Fig. 4 shows typical SEM images of these $FePO_4$ and $LiFePO_4$ samples. It was worth noting that without CNT, the resulting $FePO_4$ and $LiFePO_4$ materials still retained the morphology and structure of porous microspheres, which was almost the same with the case of $FePO_4$/CNT and $LiFePO_4$/CNT materials. This result indicated that it was the assembly of $FePO_4$ nanoparticles that was responsible for the formation of microspherical morphology during the hydrothermal process, verifying the formation mechanism of the $FePO_4$/CNT and $LiFePO_4$/CNT microspheres proposed above. Furthermore, the particle size of the $LiFePO_4$ microspheres was comparable to that of the $LiFePO_4$/CNT ones, indicating that the difference in electrochemical performance between $LiFePO_4$ and $LiFePO_4$/CNT microspheres could only result from the three-dimensional CNT network.

The microspherical morphology of the $LiFePO_4$/CNT product is beneficial to increasing its tap density. The tap density of

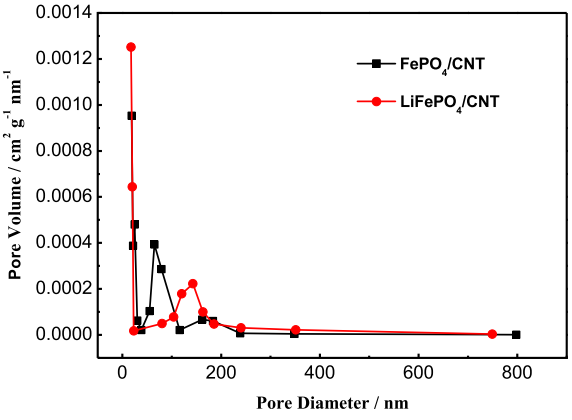

Fig. 3. Pore size distributions for the $FePO_4$/CNT and $LiFePO_4$/CNT microspheres.

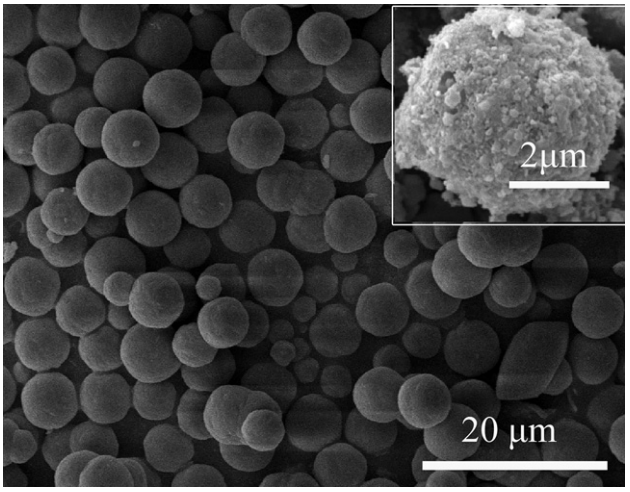

Fig. 4. SEM image of the $FePO_4$ microspheres. Inset: SEM image of the $LiFePO_4$ microspheres.

a commercial nanosized $LiFePO_4$ material, whose typical morphology is shown in Fig. 5, was less than 0.95 g cm^{-3}. However, the tap density of our $LiFePO_4$/CNT microspheres reached ~1.50 g cm^{-3}, which was slightly lower than that of the $LiFePO_4$ microspheres (1.57 g cm^{-3}) due to the incorporation of CNT. This >50% improvement would make the electrode with our $LiFePO_4$/CNT microspheres have a significantly higher volumetric energy density. Furthermore, the uniform three-dimensional CNT network is good for the electrical conductivity of the $LiFePO_4$/CNT microspheres. From the measurements using a four-point probe method, the $LiFePO_4$/CNT microspheres showed an electrical conductivity of 1.1×10^{-1} S cm^{-1}, which was ~3.4 times higher than that for $LiFePO_4$ microspheres (3.2×10^{-2} S cm^{-1}), clearly indicating that the electrical conductivity of $LiFePO_4$/CNT microspheres had been remarkably enhanced by the incorporation of CNT network.

XRD was used to detect the crystallinity information of the as-prepared $FePO_4$/CNT and $LiFePO_4$/CNT microspheres (Fig. 6). For the $FePO_4$/CNT microsphere, crystallized $FePO_4$ could be observed, confirming the formation of $FePO_4$. For the $LiFePO_4$/CNT sample, the reflection peaks could be fully ascribed to the pure orthorhombic olivine $LiFePO_4$ structure (space group: Pnma) without any impurities. Furthermore, the reflection peaks were quite narrow and

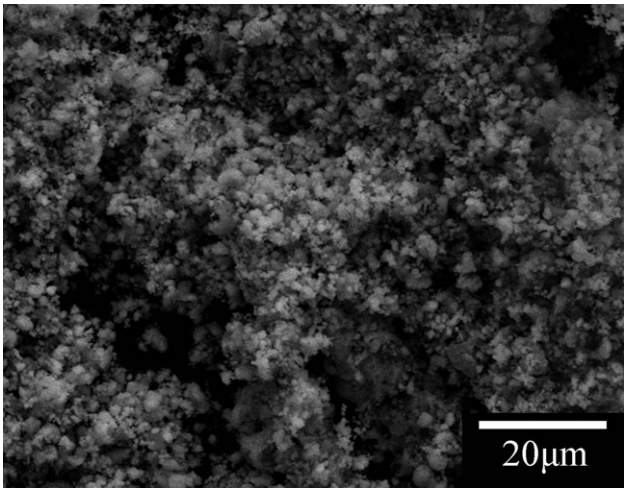

Fig. 5. SEM image of a commercial $LiFePO_4$ material.

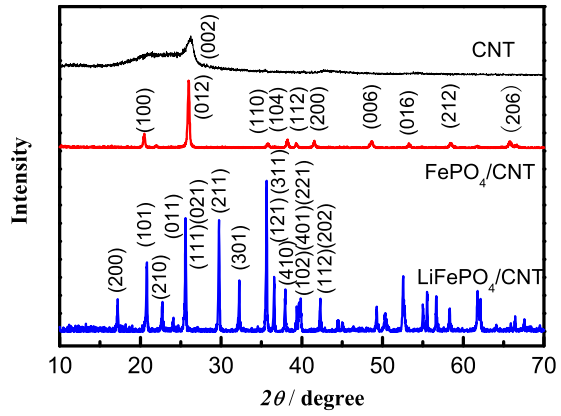

Fig. 6. XRD patterns of the CNT, $FePO_4$/CNT and $LiFePO_4$/CNT materials.

symmetric, suggesting the good crystallinity of the $LiFePO_4$ sample. Calculation of the pattern gave the lattice parameter values of $a = 5.9432$ Å, $b = 10.3046$ Å, $c = 4.6861$ Å and a unit cell volume of 286.99 Å^3, which were in good agreement with the literature values [27–29]. Although CNT alone exhibited diffraction peak corresponding to the (002) reflection at ~26.0°, they were not distinctively detected in the pattern of the $FePO_4$/CNT and $LiFePO_4$/CNT samples, which was probably due to the low CNT content.

Electrochemical Li^+ insertion/extraction properties of the $LiFePO_4$-CNT microspheres was evaluated by galvanostatic charge and discharge tests in the voltage range of 2.5–4.2 V. For comparison, the $LiFePO_4$ microspheres without CNT embedded and the $LiFePO_4$-CNT material that was prepared by mechanically mixing $LiFePO_4$ microspheres and CNT were also tested. The charge/discharge profiles for the $LiFePO_4$/CNT, $LiFePO_4$ microspheres and the $LiFePO_4$/CNT composite material (Fig. 7A) exhibited perfect voltage plateaus around 3.4 V, corresponding to the two-phase reaction between $LiFePO_4$ and $FePO_4$. However, compared with the $LiFePO_4$ microspheres and the $LiFePO_4$-CNT material, the polarization difference between the charge and discharge plateaus for the $LiFePO_4$/CNT material was lower, indicating the improved electronic and/or Li^+ conductivity. For this reason, the $LiFePO_4$/CNT microspheres delivered a gravimetric discharge capacity of 142 and 121 mAh g^{-1} at the current rates of 1C and 5C, respectively, which was significantly higher than that obtained for the $LiFePO_4$ (130 and 101 mAh g^{-1}) and the $LiFePO_4$-CNT (133 and 106 mAh g^{-1}) counterparts. From the differential capacity curves (Fig. 7B), a pair of well-defined redox peaks was observed in the range of 3.2–3.70 V, which should be attributed to the Fe^{2+}/Fe^{3+} redox couple reaction between $LiFePO_4$ and $FePO_4$ (corresponding to the Li^+ extraction and insertion). Small potential difference between the anodic and cathodic peaks demonstrates good reversibility of the charge/discharge processes. Apparently, the peak potential difference for the $LiFePO_4$/CNT microspheres was always lower than that for the $LiFePO_4$ microspheres and the $LiFePO_4$-CNT material, especially at high current rates, suggesting that the reversibility of the $LiFePO_4$/CNT microspheres was enhanced.

The volumetric specific capacity of our $LiFePO_4$/CNT microspheres was further evaluated by comparing to the commercial nanosized $LiFePO_4$ material. These volumetric specific capacity values (mAh cm^{-3}) were calculated by multiplying the gravimetric specific capacity (mAh g^{-1}) by the volumetric loading density of active materials (g cm^{-3}). As shown in Fig. 7C, much higher volumetric specific capacity was definitely achieved for the $LiFePO_4$/CNT microspheres even in the case of high-rate discharge (>155 mAh cm^{-3} at 5C). This enhanced volumetric performance could be clearly ascribed to the porous spherical morphology and

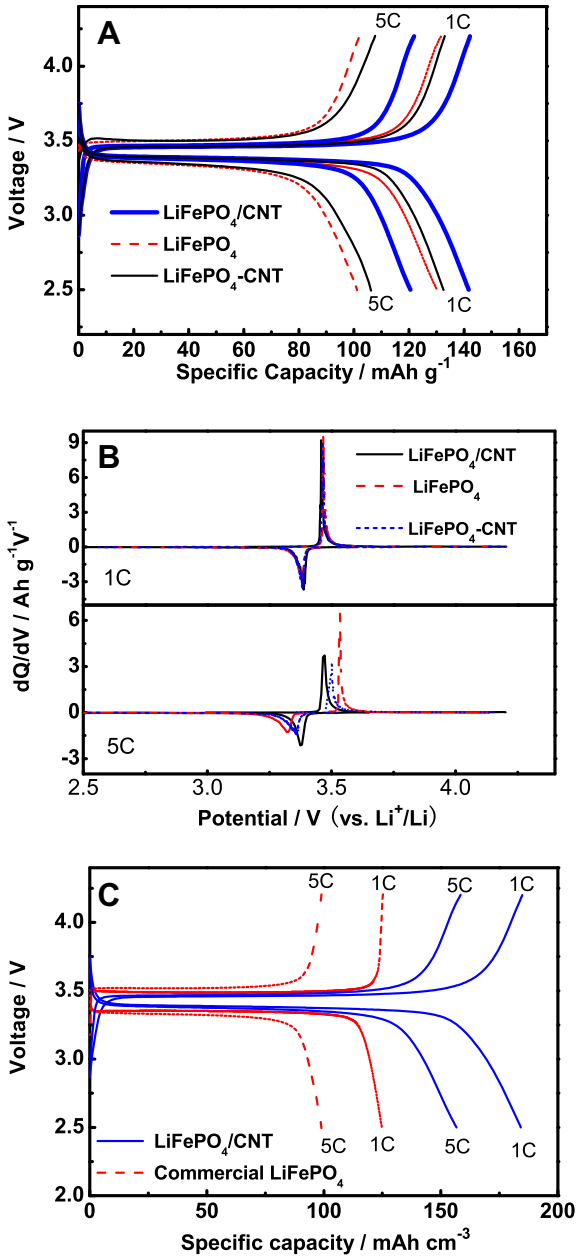

Fig. 7. (A) Charge and discharge profiles and (B) differential capacity curves of the $LiFePO_4$, $LiFePO_4$/CNT and $LiFePO_4$-CNT materials, and (C) volumetric performance of the $LiFePO_4$/CNT microspheres and the commercial $LiFePO_4$.

the highly conductive CNT network, indicating that the $LiFePO_4$/CNT material is promising for high-performance LIBs with enhanced volumetric energy density and power capability.

Rate performance and cyclability of the $LiFePO_4$/CNT microspheres were examined at various current rates ranging from 0.1C to 10C (Fig. 8A). At 0.1C rate, the $LiFePO_4$/CNT microspheres displayed a discharge capacity of 154 mAh g^{-1}, which was higher than the $LiFePO_4$ counterpart (145 mAh g^{-1}). At higher rates, the superior capacity characteristic of the $LiFePO_4$/CNT microspheres was even more apparent. Its discharge capacity at 10C was still over 104 mAh g^{-1}, whereas that for the $LiFePO_4$ material was just 77 mAh g^{-1}. To the best of our knowledge, this is among the highest performances for microspherical $LiFePO_4$ cathode material reported so far. More importantly, the $LiFePO_4$/CNT microspheres also exhibited excellent cyclic performance with no significant fade

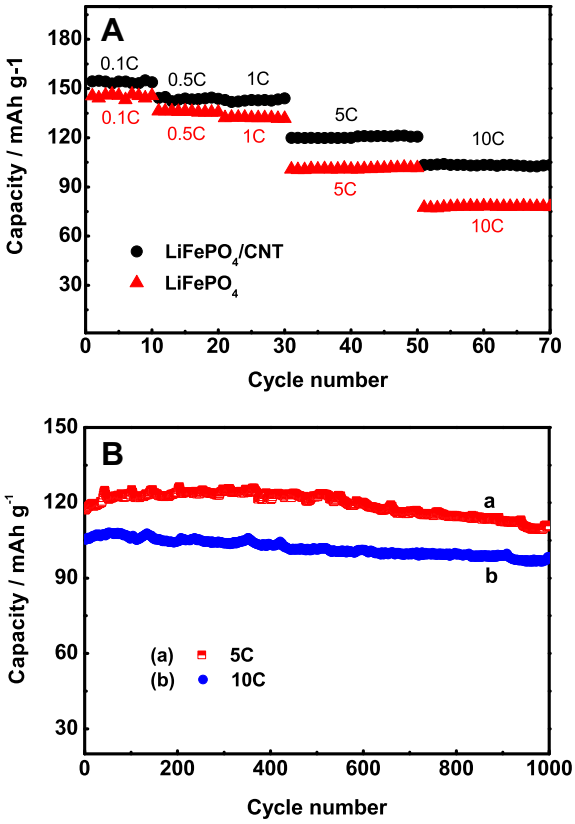

Fig. 8. (A) Cyclic performance for the $LiFePO_4$/CNT and $LiFePO_4$ microspheres at various current rates, and (B) long-term stability for the $LiFePO_4$/CNT microspheres at high current rates.

in capacity at all current rates. We also performed long-term cycling tests for the $LiFePO_4$/CNT microspheres (Fig. 8B). Our $LiFePO_4$/CNT microspheres exhibited good stability in the long-term cycling at high current rates. After 1000 cycles, the $LiFePO_4$/CNT microspheres still delivered discharge capacity of $\sim$100 mAh g^{-1} at the 10C rate, corresponding to $\sim$94% of the capacity retention. Such outstanding stability suggested that the structural integrity of the $LiFePO_4$/CNT microspheres was maintained even after high-rate charge and discharge, which was critical to many high power applications.

To analyze the effect of the conductive CNT network embedded, EIS measurement was carried out. Fig. 9 shows the EIS results for the $LiFePO_4$/CNT and $LiFePO_4$ microspheres. These impedance

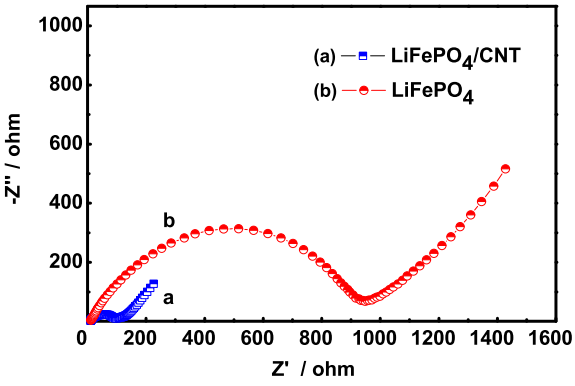

Fig. 9. Impedance spectra for the $LiFePO_4$/CNT and $LiFePO_4$ microspheres at open circuit voltage.

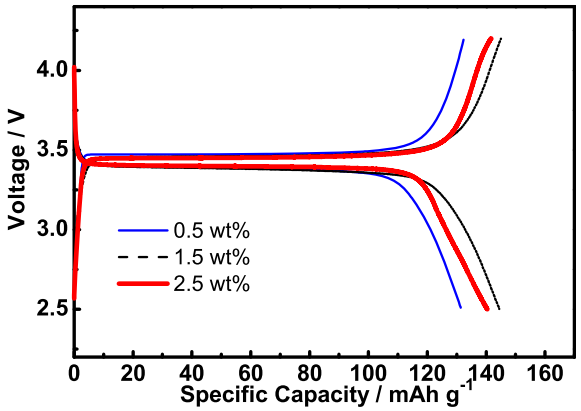

Fig. 10. Galvanostatic charge and discharge profiles for the $LiFePO_4$/CNT materials with various CNT contents.

spectra were combinations of a depressed semicircle in the high-frequency region and a straight line in the low-frequency region. The semicircle is mainly related to the charge-transfer resistance and the corresponding capacitances at the electrode/electrolyte interface [30–33]. Clearly, the $LiFePO_4$/CNT microspheres had much smaller semicircle than the $LiFePO_4$ material, indicating that the electrons and Li^+ can transfer more quickly for the $LiFePO_4$/CNT microsphere material. This result correlated well with the discharge capacity and cycle stability of the $LiFePO_4$/CNT microspheres, which should be attributed to the highly conductive CNT network that (a) improved the electrical conductivity and contact of $LiFePO_4$ spheres, and (b) led to a porous structure for convenient electrolyte penetration and fast ionic diffusion.

In order to investigate the influence of CNT content on the electrochemical performance of the $LiFePO_4$/CNT microspheres, the galvanostatic charge/discharge curves for the $LiFePO_4$/CNT microspheres with various CNT contents are compared in Fig. 10. All the samples exhibited a flat voltage plateau and excellent reversibility. With an increase in the CNT content from 0.5 to 1.5 wt %, the reversible discharge capacity of the $LiFePO_4$/CNT microspheres was improved from 132 to 145 mAh g^{-1}, which demonstrated that higher CNT contents would bring better electronic conductivity, and thus higher reversibility. However, at 2.5 wt % of CNT content, the discharge capacity dropped to around 140 mAh g^{-1}, which could be ascribed to the fact that excessive CNT substituted too much $LiFePO_4$ and resulted the decrease of theoretic capacity. Thus, the $LiFePO_4$/CNT microspheres with $\sim$1.5 wt% of CNT content was the optimum, which exhibited well discharge capacity and rate performance.

4. Conclusions

In summary, we report the design and facile preparation of porous $FePO_4$/CNT microspheres by an in-situ CNT-embedding approach that involves a hydrothermal process. Using the $FePO_4$/CNT microspheres as precursor, $LiFePO_4$/CNT microspheres were obtained by chemical lithiation. The $FePO_4$/CNT and $LiFePO_4$/CNT microspheres contain uniform and well-connected CNT networks, which remarkably improve the electronic conductivity. Meanwhile, these materials possess abundant nanopores that provide large surface area and favored electrolyte irrigation. Thus, by combining high tap density and improved electronic and ionic conductivity, quite high volummetric energy density and rate capacity are simultaneously achieved for the $LiFePO_4$/CNT microspheres. Their initial reversible capacity reaches 104 mAh g^{-1} at a current rate of 10C, and the capacity retention is

over 94% after 1000 cycles. This $LiFePO_4$/CNT material and its facile preparation method are rather promising for high power LIBs with desirable volumetric energy density in electric vehicles. Such a approach can also be extended to other electrode materials.

Acknowledgments

This work was supported by National High Technology Research and Development Program (863 Program) of China (no. 2012AA110203).

References

[1] J.M. Tarascon, M. Armand, Nature 414 (2001) 359–367.
[2] S.I. Nishimura, G. Kobayashi, K. Ohoyama, J. Kanno, M. Yashima, A. Yamada, Nature Materials 7 (2008) 707–711.
[3] A.K. Padhi, K.S. Nanjundaswamy, J.B. Goodenough, Journal of the Electrochemical Society 144 (1997) 1188–1194.
[4] J. Wang, X. Sun, Energy & Environmental Science 5 (2012) 5163–5185.
[5] D.D. MacNeil, Z. Lu, Z. Chen, J.R. Dahn, Journal of Power Sources 108 (2002) 8–14.
[6] A.S. Andersson, J.O. Thomas, B. Kalska, L. Haggstrom, Electrochemical and Solid State Letters 3 (2000) 66–68.
[7] Z. Chen, J.R. Dahn, Journal of the Electrochemical Society 149 (2002) A1184–A1189.
[8] S.Y. Chung, J.T. Bloking, Y.M. Chiang, Nature Materials 1 (2002) 123–128.
[9] G.X. Wang, S. Bewlay, J. Yao, J.H. Ahn, H.K. Liu, S.X. Dou, Electrochemical and Solid State Letters 7 (2004) A503–A506.
[10] J.K. Kim, G. Cheruvally, J.H. Ahn, H.J. Ahn, Journal of Physics and Chemistry of Solids 69 (2008) 1257–1260.
[11] A.A. Salah, A. Mauger, K. Zaghib, J.B. Goodenough, N. Ravet, M. Gauthier, F. Gendron, C.M. Julien, Journal of the Electrochemical Society 153 (2006) A1692–A1701.
[12] P. Gibot, M. Casas-Cabanas, L. Laffont, S. Levasseur, P. Carlach, S. Hamelet, J.-M. Tarascon, C. Masquelier, Nature Materials 7 (2008) 741–747.
[13] H. Huang, S. Yin, L. Nazar, Electrochemical and Solid State Letters 4 (2001) A170–A172.
[14] S.B. Lee, S.H. Cho, S.J. Cho, G.J. Park, S.H. Park, Y.S. Lee, Electrochemistry Communications 10 (2008) 1219–1221.
[15] H.M. Xie, R.S. Wang, J.R. Ying, L.Y. Zhang, A.F. Jalbout, H.Y. Yu, G.L. Yang, X.M. Pan, Z.M. Su, Advanced Materials 18 (2006) 2609–2613.
[16] D.H. Kim, J. Kim, Electrochemical and Solid State Letters 9 (2006) A439–A442.
[17] Y. Wang, Y. Wang, E. Hosono, K. Wang, H. Zhou, Angewandte Chemie International Edition 47 (2008) 7461–7465.
[18] S.W. Oh, S. Myung, S.M. Oh, K.H. Oh, K. Amine, B. Scrosati, Y.K. Sun, Advanced Materials 22 (2010) 4842–4845.
[19] C.M. Doherty, R.A. Caruso, C.J. Drummond, Energy & Environmental Science 3 (2010) 813–823.
[20] J. Ying, M. Lei, C. Jiang, C. Wan, X. He, J. Li, L. Wang, J. Ren, Journal of Power Sources 158 (2006) 543–549.
[21] M.R. Yang, T.H. Teng, S.H. Wu, Journal of Power Sources 159 (2006) 307–311.
[22] F. Yu, J. Zhang, Y. Yang, G. Song, Journal of Materials Chemistry 19 (2009) 9121–9125.
[23] J. Chen, C. Hsu, Y. Lin, M. Hsiao, G. Fey, Journal of Power Sources 184 (2008) 498–502.
[24] C. Gao, C.D. Vo, Y.Z. Jin, W.W. Li, S.P. Armes, Macromolecules 38 (2005) 8634–8648.
[25] B. Zhu, X. Li, Z. Wang, H. Guo, Materials Chemistry and Physics 98 (2006) 373–376.
[26] L. Wang, G.C. Liang, X.Q. Ou, X.K. Zhi, J.P. Zhang, J.Y. Cui, Journal of Power Sources 189 (2009) 423–428.
[27] X. Wu, L. Jiang, F. Cao, Y. Guo, L. Wan, Advanced Materials 21 (2009) 2710–2714.
[28] A.S. Andersson, B. Kalska, L. Haggstrom, J.O. Thomas, Solid State Ionics 130 (2000) 41–52.
[29] J. Zheng, X. Li, Z. Wang, H. Guo, S. Zhou, Journal of Power Sources 184 (2008) 574–577.
[30] X.Z. Liao, Z.F. Ma, Y.S. He, X.M. Zhang, L. Wang, Y. Jiang, Journal of the Electrochemical Society 152 (2005) A1969–A1973.
[31] X.J. Chen, G.S. Cao, X.B. Zhao, J.P. Tu, T.J. Zhu, Journal of Alloys and Compounds 463 (2008) 385–389.
[32] J.Y. Xiang, J.P. Tu, L. Zhang, X.L. Wang, Y. Zhou, Y.Q. Qiao, Y. Lu, Journal of Power Sources 195 (2010) 8331–8335.
[33] T. Muraliganth, A. Murugan, A. Manthiram, Journal of Materials Chemistry 18 (2008) 5661–5668.